

# Effect of $\text{SnO}_2$ on improvement on the microwave dielectric properties of $\text{Ba}_2\text{Ti}_9\text{O}_{20}$

Chi-Ben Chang · Keh-Chyang Leou · Wen-Yang Shu ·  
I-Nan Lin

Received: 31 July 2005 / Accepted: 26 December 2006 / Published online: 13 March 2007  
© Springer Science + Business Media, LLC 2007

**Abstract** Effect of  $\text{SnO}_2$  addition on the crystal structure/microstructure and the related microwave dielectric properties of the  $\text{Ba}_2\text{Ti}_9\text{O}_{20}$  were systematically investigated. Incorporation of  $\text{SnO}_2$  markedly stabilized the phase constituent and microstructure for the  $\text{Ba}_2\text{Ti}_9\text{O}_{20}$  such that high quality materials can be obtained in a much wider processing window. The sintered density of the  $\text{Ba}_2\text{Ti}_9\text{O}_{20}$  increased linearly, but the microwave dielectric constant ( $K$ ) decreased monotonically, with the  $\text{SnO}_2$  doping concentration. The quality factor ( $Q_{xf}$ ) of the materials increased firstly due to the addition of  $\text{SnO}_2$ , but decreased slightly with further increase in  $\text{SnO}_2$  content. The best microwave dielectric properties obtained are  $K=38.5$  and  $Q_{xf}=31,500$  GHz, which occurs for the 0.055 mol  $\text{SnO}_2$ -doped and 1350 °C/4 h sintered samples. These properties are markedly better than those for undoped materials ( $K=38.8$  and  $Q_{xf}=26,500$  GHz).

**Keywords** Microwave dielectrics ·  $\text{SnO}_2$  ·  $\text{ZrO}_2$  · Mixed-oxide process

---

C.-B. Chang · K.-C. Leou  
Department of Engineering and System Science,  
National Tsing-Hua University,  
Hsinchu, Taiwan 300, Republic of China

W.-Y. Shu  
Materials & Electro-Optics Research Division,  
Chung-Shan Institute of Science & Technology,  
Lung-Tan, Taiwan, Republic of China

I.-N. Lin (✉)  
Department of Physics, Tamkang University,  
Tamsui 251 Taiwan, Republic of China  
e-mail: inanlin@mail.tku.edu.tw

## 1 Introduction

$\text{Ba}_2\text{Ti}_9\text{O}_{20}$  phase was first reported by Jerker and Kwestroo in  $\text{BaO}-\text{TiO}_2-\text{SnO}_2$  ternary system [1]. O'Bryan et al. [2] showed that it possess marvelous microwave dielectric properties, including high dielectric constant and large quality factor. Since then the modification on microwave properties of  $\text{Ba}_2\text{Ti}_9\text{O}_{20}$  materials via the addition of dopants [3–7] was widely investigated. However, the reported results are quite controversial, which is mainly due to the difficulty in forming single-phase Hollandite-like structured  $\text{Ba}_2\text{Ti}_9\text{O}_{20}$ . Secondary phases, such as  $\text{BaTi}_4\text{O}_9$  or  $\text{BaTi}_5\text{O}_{11}$ , were observed to form preferentially in the calcinations of  $\text{BaO}-\text{TiO}_2$  mixture [8] that hinder the formation of Hollandite-like structured  $\text{Ba}_2\text{Ti}_9\text{O}_{20}$  phase. Co-precipitation process, which mixes the cations in atomic scale, can produce multiple-metallic-oxides with better homogeneity and higher activity [9–13]. However, the stoichiometry control in co-precipitation process is the difficult, as this process is sensitive to the pH-value and temperature.

In this paper, we utilized the nano-sized  $\text{BaTiO}_3$  and  $\text{TiO}_2$  powders as starting material to circumvent the difficulty due to the presence of intermediate phase. Moreover, the  $\text{ZrO}_2$  and  $\text{SnO}_2$  additives, which are isovalent with  $\text{TiO}_2$  species, were incorporated into the materials, for the purpose of stabilizing the characteristics of the  $\text{Ba}_2\text{Ti}_9\text{O}_{20}$ .

## 2 Experimental

Nano-sized  $\text{BaTiO}_3$  powders (50 nm) were mixed with nano-sized Anatase  $\text{TiO}_2$  powders (~40 nm) in a nominal composition of  $\text{Ba}_2\text{Ti}_9\text{O}_{20}$ . The mixtures were calcined at

1,000 °C for 4 h in air, followed by pulverization–granulation–pelletization processes and were then sintered at 1,200–1,380 °C for 4 h in air. The microstructure of the sintered samples was examined using scanning electron microscopy (SEM)(Joel 6700F). The crystal structure of the calcined powders and sintered samples was examined using X-ray diffractometry (XRD) (Rigaku D/max-II). The density of the sintered materials was measured using Archimedes method. The microwave dielectric constant ( $K$ ) and Qxf-value of the  $\text{Ba}_2\text{Ti}_9\text{O}_{20}$  samples were measured using a cavity method at 3–4 GHz [14]. The rod-shaped samples were placed at the center of the metallic cavity by using a quartz stand (~5 mm in diameter & 5 mm height). The inner wall of the metallic cavity was coated with Au. The microwave dielectric properties were estimated from the resonance peaks acquired by a HP 8722 network analyzer.

### 3 Results and discussion

Even when the nano-sized  $\text{BaTiO}_3/\text{TiO}_2$  powders were used as starting material for the preparation of  $\text{Ba}_2\text{Ti}_9\text{O}_{20}$ , the  $\text{BaTi}_4\text{O}_9$  phase still formed preferentially during the calcinations process. Thus formed  $\text{BaTi}_4\text{O}_9$  intermediate phase will react further with the residual  $\text{TiO}_2$  (rutile) and be converted into Hollandite-like  $\text{Ba}_2\text{Ti}_9\text{O}_{20}$  phase, when the samples were sintered at a temperature higher than 1,250 °C (4 h), as shown in Fig. 1a. No residual secondary phase was observed. Such a temperature is lower than the one usually required to form pure Hollandite-like phase from the  $\text{BaCO}_3+\text{TiO}_2$  mixture. The formation of Hollandite-like phase is facilitated due to the utilization of nano-sized powders. Such a phenomenon can be ascribed to the fact that the size of the starting powder mixture,  $\text{BaTiO}_3+\text{TiO}_2$ , the preferentially formed  $\text{BaTi}_4\text{O}_9$  aggregates is very small. This facilitates the interdiffusion between the  $\text{BaTi}_4\text{O}_9$  and  $\text{TiO}_2$  phases and enhances the phase transformation kinetics.

The density of the materials increases with sintering temperature, reaching 98% theoretical density (T.D.), when sintered at 1,350 °C (4 h) and then decreases slightly when the sintering temperature increases further to 1,380 °C (4 h) as shown in curve I in Fig. 2a. The  $K$ -value of these materials also increases with sintering temperature firstly up to 1,350 °C (4 h) and decreases slightly when sintered at 1,380 °C (4 h) (curve I, Fig. 2b). The quality factor (Qxf) of the materials changes with the sintering temperature even more, the Qxf-value increases monotonously from 23,200 to 26,500 GHz as the sintering temperature increases from 1,250 °C (4 h) to 1,350 °C (4 h). But it drops abruptly to 10,000 GHz for 1,380 °C (4 h)-sintered samples (curve I, Fig. 2c). The microwave dielectric properties of the

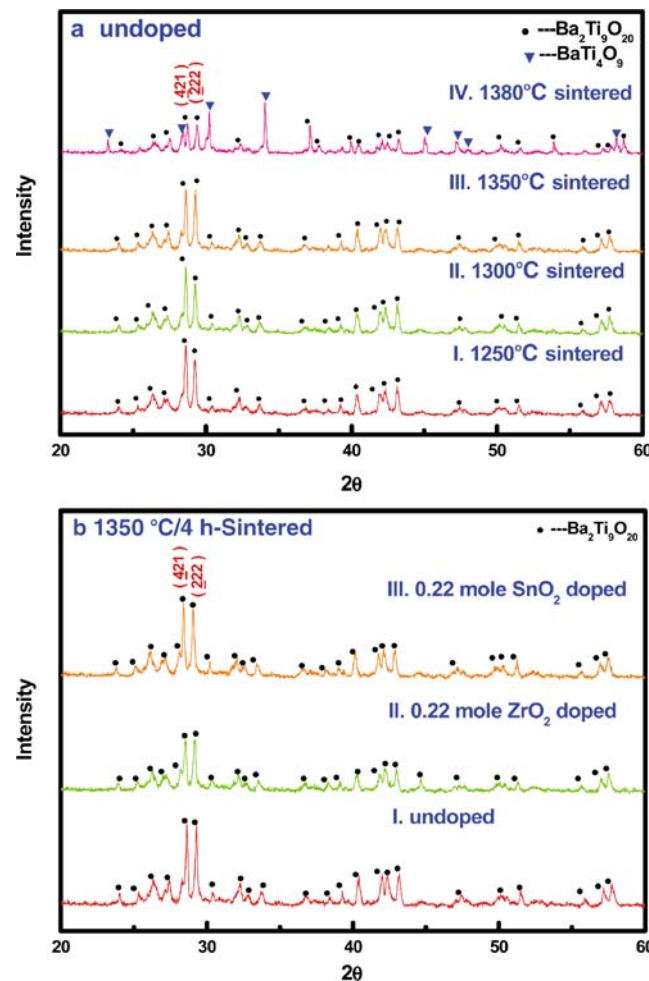


**Fig. 1** X-ray diffraction patterns of **a** the undoped  $\text{Ba}_2\text{Ti}_9\text{O}_{20}$  materials sintered at 1,250–1,350 °C (4 h) and **b** the  $\text{Ba}_2(\text{Ti}_{9-x}\text{M}_x)\text{O}_{20}$  materials, which are either undoped ( $x=0$ ),  $\text{ZrO}_2$  or  $\text{SnO}_2$  incorporated ( $x=0.22$ ) and were sintered at 1,350 °C (4 h); the Miller index corresponding to  $2\theta=28.5$  and  $29.1^\circ$  are (421) and (222), respectively

$\text{Ba}_2\text{Ti}_9\text{O}_{20}$  materials correlate intimately with their density and sintering at too high temperature (1,380 °C (4 h)) markedly degrades these characteristics.

To understand the true factor for degrading the quality for the 1,380 °C (4 h)-sintered samples, the microstructure of these samples was examined. Figure 3a clearly shows that the samples sintered at 1,350 °C (4 h) possess a bimodal microstructure, i.e., they contain rod-shaped grains about  $1\times 4 \mu\text{m}$  in size distributed among fine equi-axed grains about  $0.3 \mu\text{m}$  in size. Large elongated grains about  $10\times 4 \mu\text{m}$  in size are observed occasionally (circled, Fig. 3a). Inset of Fig. 3a illustrates that the abnormal grain growth phenomenon occurs even more effectively for the 1,380 °C (4 h)-sintered samples. These results indicate that, although the utilization of nano-sized  $\text{BaTiO}_3$  and  $\text{TiO}_2$  as starting materials facilitates the phase transformation of the materials, the preparation of  $\text{Ba}_2\text{Ti}_9\text{O}_{20}$  is still complicated

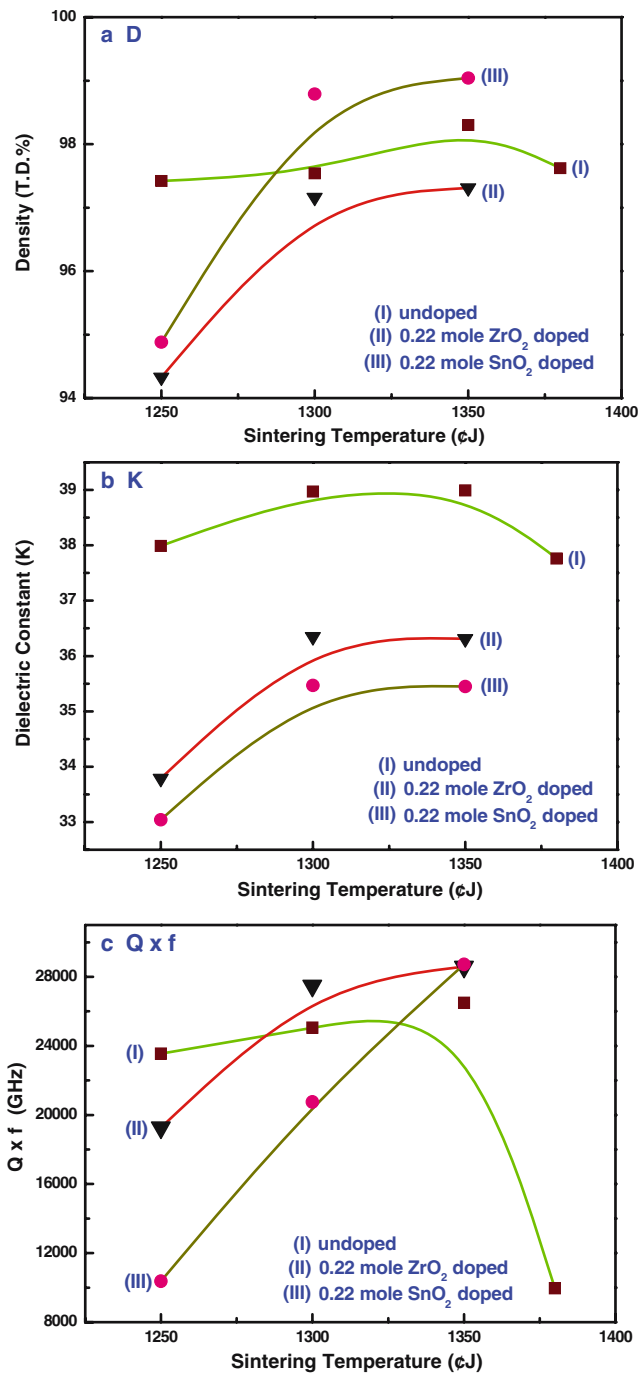


**Fig. 2** The **a** sintered density, **D**, **b** dielectric constant, *K*, and **c** quality factor, *Qxf*-value, for the  $\text{Ba}_2\text{Ti}_9\text{O}_{20}$  materials sintered at 1,250–1,380 °C (4 h): (I) undoped, (II) 0.22 mol  $\text{ZrO}_2$ -incorporated and (III) 0.22 mol  $\text{SnO}_2$ -incorporated

due to the preferential formation of  $\text{BaTi}_4\text{O}_9$  as intermediate phase. Even though such a preferentially formed  $\text{BaTi}_4\text{O}_9$  can be transformed into Hollandite-like phase during sintering process, the reaction of the  $\text{BaTi}_4\text{O}_9$  phase with the residue  $\text{TiO}_2$  will induce heat locally, which potentially induces the abnormal grain growth phenomenon. To confirm such a proposed model, the reaction process

between  $\text{BaTi}_4\text{O}_9$  &  $\text{TiO}_2$  mixture was examined by using differential scanning calorimetry (DSC) and the results are shown in Fig. 4. These figures indicate clearly that, while only endothermic reactions were observed below 1,200.0 °C, there exist two exothermic reactions at 1,250.5 and 1,270.5 °C.

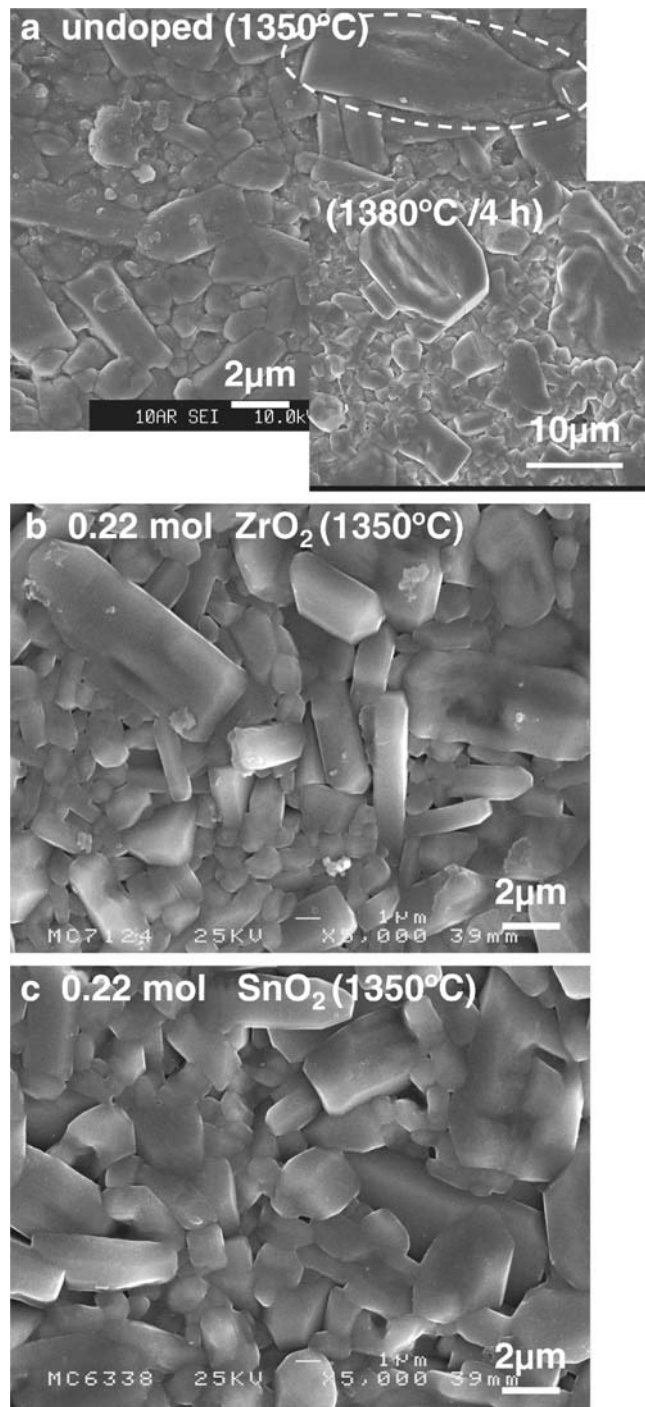


**Fig. 3** SEM micrographs for the  $\text{Ba}_2\text{Ti}_9\text{O}_{20}$  materials sintered at 1,350 °C (4 h): **a** undoped, **b** 0.22 mol  $\text{ZrO}_2$ -incorporated and **c** 0.22 mol  $\text{SnO}_2$ -incorporated; the inset in **a** is the micrographs for the 1,380 °C-sintered undoped- $\text{Ba}_2\text{Ti}_9\text{O}_{20}$  materials

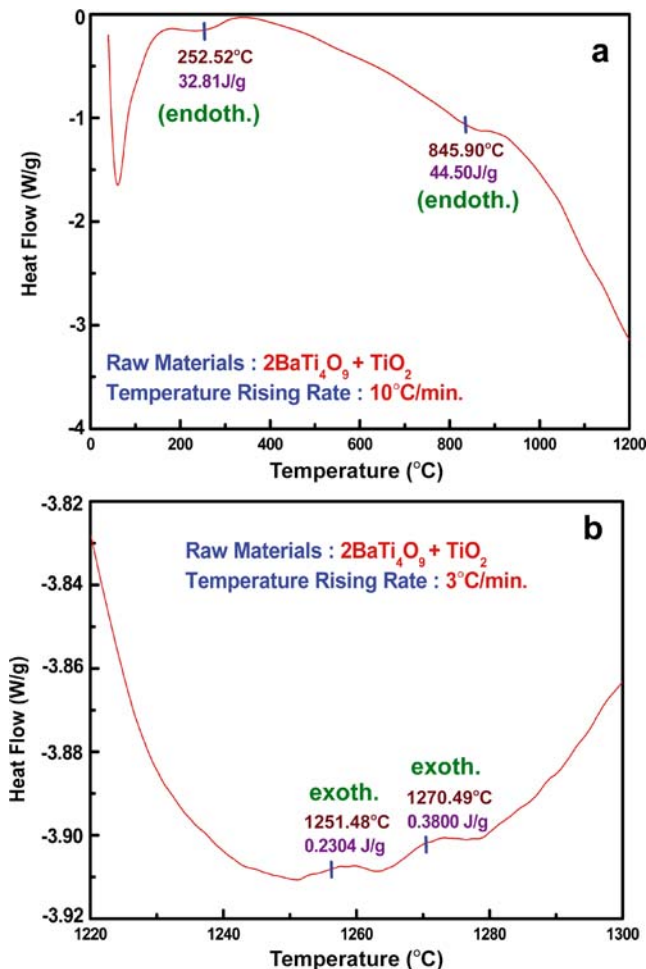


**Fig. 4** The reaction sequence of heating the  $\text{Ba}_2\text{Ti}_9\text{O}_{20} + \text{TiO}_2$  mixture, showing the existence of the exothermic reaction at 1,251.5 and 1270.5 °C

Moreover, Fig. 1a shows that the diffraction peaks of the Hollandite-like phase are broadened and there appears the  $\text{BaTi}_4\text{O}_9$  secondary phase for the 1,380 °C (4 h)-sintered samples (XRD-IV, Fig. 1a). The  $\text{BaTi}_4\text{O}_9$  phase observed in these over-fired samples is most probably resulted from the dissociation of  $\text{Ba}_2\text{Ti}_9\text{O}_{20}$  phase rather than the incomplete phase transformation process. The induction of secondary phase is presumed to be the main cause resulting in detrimental effect on the Qxf-factor of these samples. Therefore, the approach of sintering the materials at higher temperature for increasing the density of the samples so as to improve the microwave dielectric properties of the  $\text{Ba}_2\text{Ti}_9\text{O}_{20}$  materials is not practical, as it will induce the dissociation of  $\text{Ba}_2\text{Ti}_9\text{O}_{20}$  phase.

To enhance the *reaction kinetics* and hence to improve the characteristics for the  $\text{Ba}_2\text{Ti}_9\text{O}_{20}$ , small amount of additives such as  $\text{Sn}^{4+}$ - or  $\text{Zr}^{4+}$ -species, which are iso-valent to  $\text{Ti}^{4+}$ -species, were incorporated into these materials to modify the development of granular structure. Figure 2a reveals that, when the samples were densified at 1,350 °C (4 h), with

addition of  $\text{ZrO}_2$  (0.22 mol) to replace for the  $\text{TiO}_2$  lowers the sintered density for the materials (curve II). However incorporation of  $\text{SnO}_2$  (0.22 mol) increases it appreciably (curve III). Both  $\text{ZrO}_2$  and  $\text{SnO}_2$ -doping markedly lowers the *K*-value of the  $\text{Ba}_2\text{Ti}_9\text{O}_{20}$  materials, i.e., the *K*-value is around 35.5–36.2 for the  $\text{ZrO}_2$  (or  $\text{SnO}_2$ )-doped materials (curves II & III, Fig. 2b) and 39 for undoped ones (curves I, Fig. 2b). However,  $\text{ZrO}_2$  (or  $\text{SnO}_2$ )-doping appreciably improves the Qxf-value for the  $\text{Ba}_2\text{Ti}_9\text{O}_{20}$  materials. When they were sintered at 1,350 °C (4 h), i.e., Qxf factor is ~29,000 GHz for  $\text{ZrO}_2$  (or  $\text{SnO}_2$ )-doped materials (curves II & III, Fig. 2c) and is ~26,500 GHz for undoped samples (curves I, Fig. 2c).

Figure 3b and c show the SEM micrographs of the 1,350 °C/4 h-sintered samples, which were doped with  $\text{ZrO}_2$  and  $\text{SnO}_2$ , respectively. These figures reveal that  $\text{ZrO}_2$  (or  $\text{SnO}_2$ ) doping results in more uniform granular structure, as compared with that of the un-doped ones. The bimodal microstructure occurred in the undoped samples was no longer observed for the  $\text{ZrO}_2$  (or  $\text{SnO}_2$ ) doped samples. These results imply that, for the samples possessing high sintered density and pure Hollandite-like phased  $\text{Ba}_2\text{Ti}_9\text{O}_{20}$  materials, uniformity in granular structure is another important factor responsible for improving the quality factor of the materials.

The incorporation of  $\text{ZrO}_2$  (or  $\text{SnO}_2$ ) species insignificantly alters the average grain size of the  $\text{Ba}_2\text{Ti}_9\text{O}_{20}$  materials, i.e., the average grain size for the samples is about  $1.6 \times 5 \mu\text{m}$ , regardless of whether they were  $\text{ZrO}_2$ - (or  $\text{SnO}_2$ )-doped or undoped ones. Apparently, the beneficial effect of the incorporation of  $\text{ZrO}_2$  (or  $\text{SnO}_2$ ) species on improving the Qxf-value for the  $\text{Ba}_2\text{Ti}_9\text{O}_{20}$  materials is mainly due to the improvement on the uniformity of the granular structure, rather than the decrease in grain size. More detailed investigation reveals that,  $\text{SnO}_2$ -doping (0.22 mol) results in more uniform granular structure than the  $\text{ZrO}_2$ -doping (0.22 mol) does (Fig. 3b and c) and therefore, leads to better microwave dielectric properties. In fact, further investigation indicates that non-uniform grain growth phenomenon will also be induced when the materials contain too few proportion of  $\text{ZrO}_2$ -dopants (not shown). This non-uniform grain growth phenomenon effectively alters the Qxf-value of the  $\text{Ba}_2\text{Ti}_9\text{O}_{20}$  materials. That is,  $\text{ZrO}_2$ -doping does not consistently modify the characteristics of the  $\text{Ba}_2\text{Ti}_9\text{O}_{20}$  materials. Thereafter, only the effect of  $\text{SnO}_2$ -doping on the characteristics of the  $\text{Ba}_2\text{Ti}_9\text{O}_{20}$  materials was further investigated.

XRD patterns in Fig. 5 indicate that all the  $\text{SnO}_2$ -doped samples ( $x=0.055$ –0.22 in  $\text{Ba}_2(\text{Ti}_{9-x}\text{Sn}_x)\text{O}_{20}$ ), which were sintered at 1,250–1,350 °C for 4 h, are of pure Hollandite-like phase. No secondary phases are induced. The texture characteristics of the samples are not pronouncedly altered due to the change in  $\text{SnO}_2$ -content of sintering temperature, which is implied by the phenomenon that the (421)/(222)

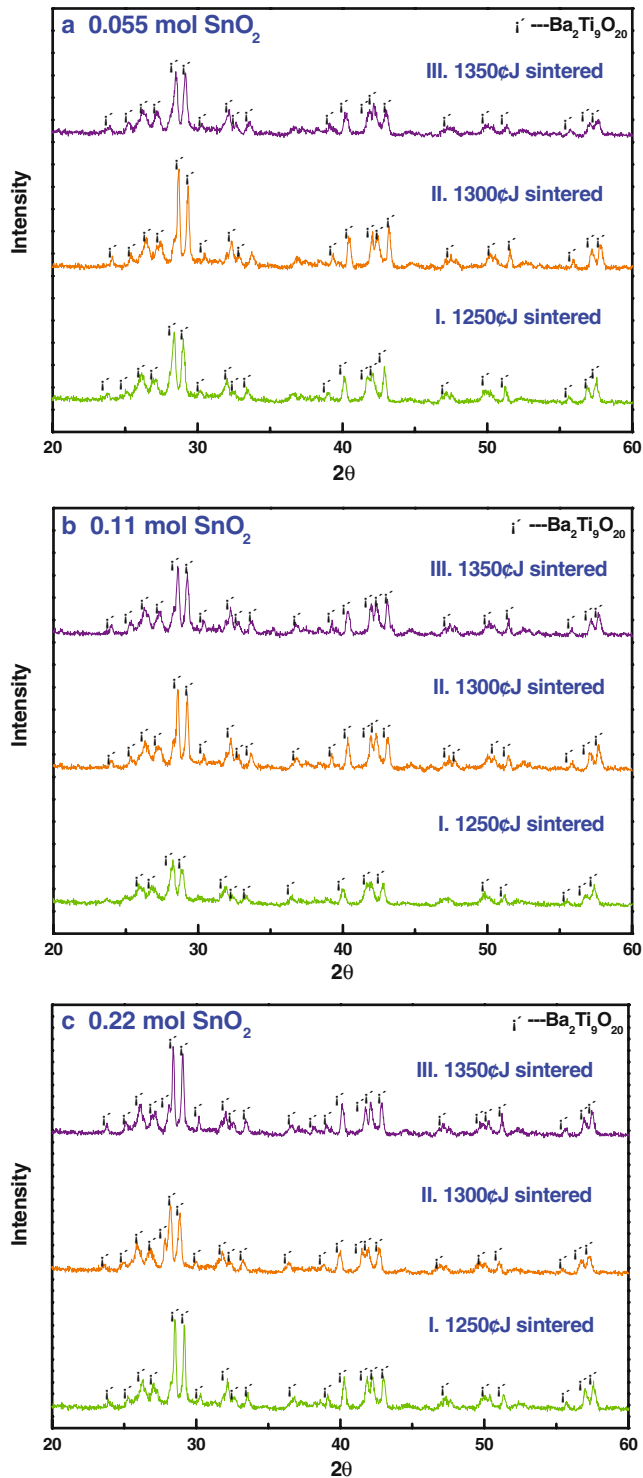


**Fig. 5** Effect of SnO<sub>2</sub> incorporation on the X-ray diffraction patterns of the Ba<sub>2</sub>(Ti<sub>9-x</sub>Sn<sub>x</sub>)O<sub>20</sub> materials sintered at 1,250–1,350 °C (4 h); the SnO<sub>2</sub> concentration ( $x$ -value) is **a** 0.055, **b** 0.11, and **c** 0.22 mol

relative peak intensity in the corresponding XRD patterns is about the same, regardless of the doping concentration and the sintering temperature.

The sintered density for the SnO<sub>2</sub>-doped Ba<sub>2</sub>Ti<sub>9</sub>O<sub>20</sub> materials increases monotonously with the sintering tem-

perature (Fig. 6a). So do the microwave dielectric properties (Fig. 6b and c). It is interesting to observe that, comparing with the undoped samples, the SnO<sub>2</sub>-doped materials densify in a lower rate when sintering at a temperature lower than 1,250 °C/4 h, but they achieve higher density when fired at higher temperature. The SnO<sub>2</sub>-added samples possess a density about 2% higher than that of the undoped Ba<sub>2</sub>Ti<sub>9</sub>O<sub>20</sub> materials, when sintered at

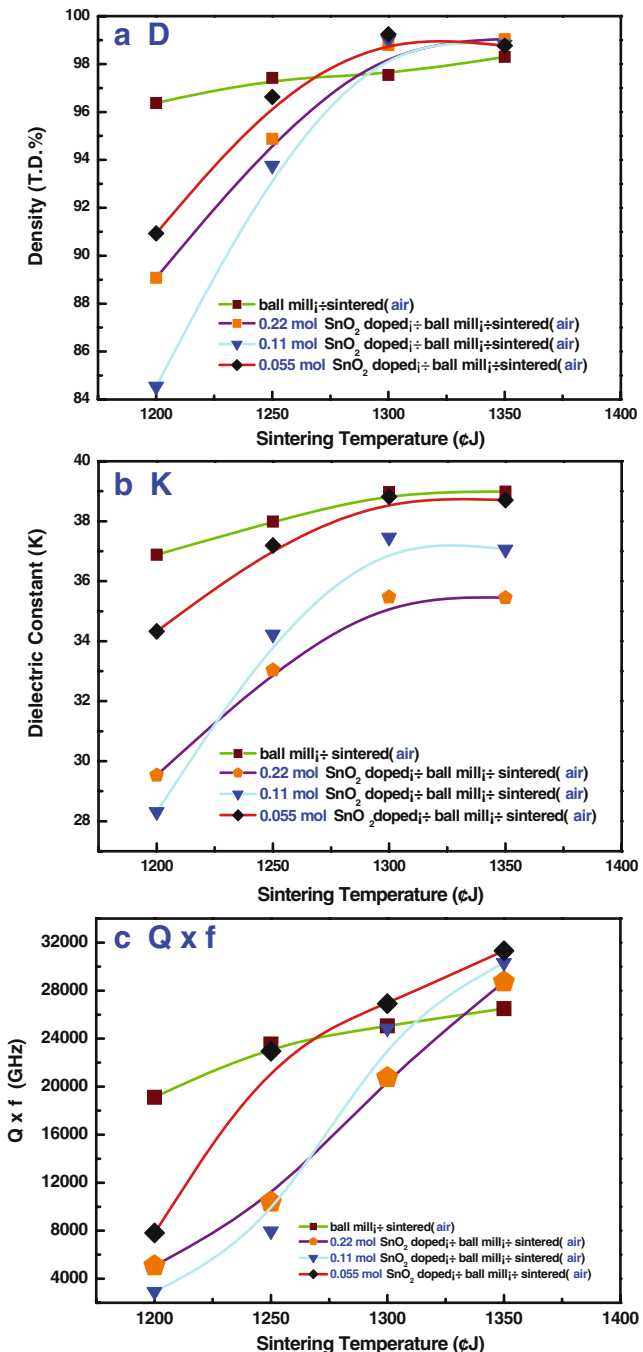


**Fig. 6** Variation of the **a** sintered density, **b** dielectric constant,  $K$ , and **c** quality factor,  $Qxf$ -value, for the Ba<sub>2</sub>(Ti<sub>9-x</sub>Sn<sub>x</sub>)O<sub>20</sub> materials with the sintering temperature (1,200–1,350 °C/4 h); the SnO<sub>2</sub> concentration ( $x$ -value) is 0.055–0.22 mol

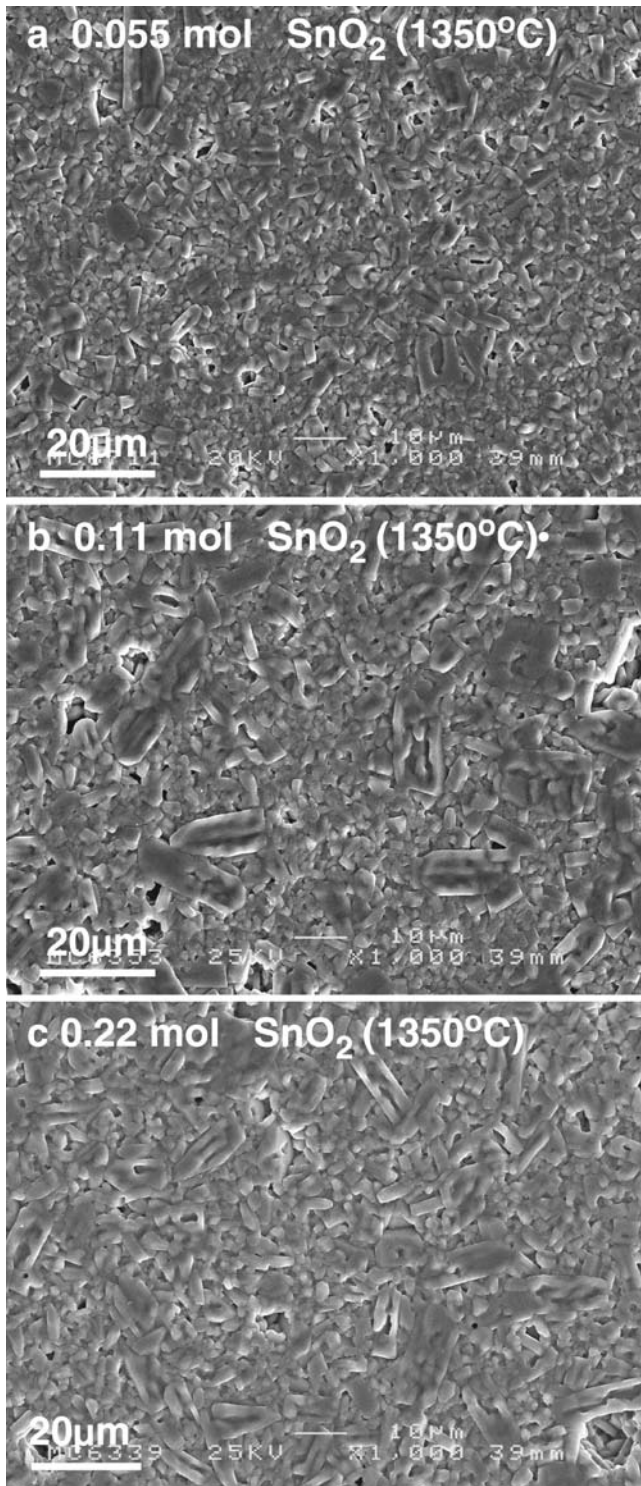


**Fig. 7** Effect of  $\text{SnO}_2$  incorporation on the SEM microstructure of the  $\text{Ba}_2(\text{Ti}_{9-x}\text{Sn}_x)\text{O}_{20}$  materials sintered at  $1,350\text{ }^\circ\text{C}$  (4 h); the  $\text{SnO}_2$  concentration ( $x$ -value) is **a** 0.055, **b** 0.11, and **c** 0.22 mol

$1,350\text{ }^\circ\text{C}/4\text{ h}$ , regardless of the doping level. Such a phenomenon can be attributed to the modification on the microstructure of the grains, which will be discussed shortly.

The granular structure for  $\text{SnO}_2$ -doped  $\text{Ba}_2\text{Ti}_9\text{O}_{20}$  samples sintered at  $1,350\text{ }^\circ\text{C}$  (4 h) found quite uniform as seen in SEM micrograph in Fig. 7. Neither ultra-small grains nor the abnormally grown large grains were observed. It shows that the incorporation of  $\text{SnO}_2$  additives stabilizes the crystallization kinetics and improves the development of granular structure for the  $\text{Ba}_2\text{Ti}_9\text{O}_{20}$  materials. Detailed examination on these SEM micrographs reveals that addition of  $\text{SnO}_2$  decreases the length-to-diameter aspect ratio of the grains. Therefore, the bridging effect due to anisotropic growth of the high-aspect-ratio grains is pronouncedly suppressed such that the densification process is facilitated. All the  $\text{SnO}_2$ -doped materials possess very high density ( $>98\%\text{T.D.}$ ), when they were sintered at  $1,350\text{ }^\circ\text{C}/4\text{ h}$ .

To understand how  $\text{SnO}_2$ -addition affect the characteristics of  $\text{Ba}_2\text{Ti}_9\text{O}_{20}$  materials, the XRD patterns in Fig. 5 were analyzed in detail. Since all the  $\text{SnO}_2$ -doped materials are of pure Hollandite-like phase, the full-width at half-maximum (FWHM) of the diffraction peaks is closely related to the grain size of the materials. The variation of FWHM of the major diffraction peaks, (421) & (222), against the  $\text{SnO}_2$  doping concentration is shown in Fig. 8a.

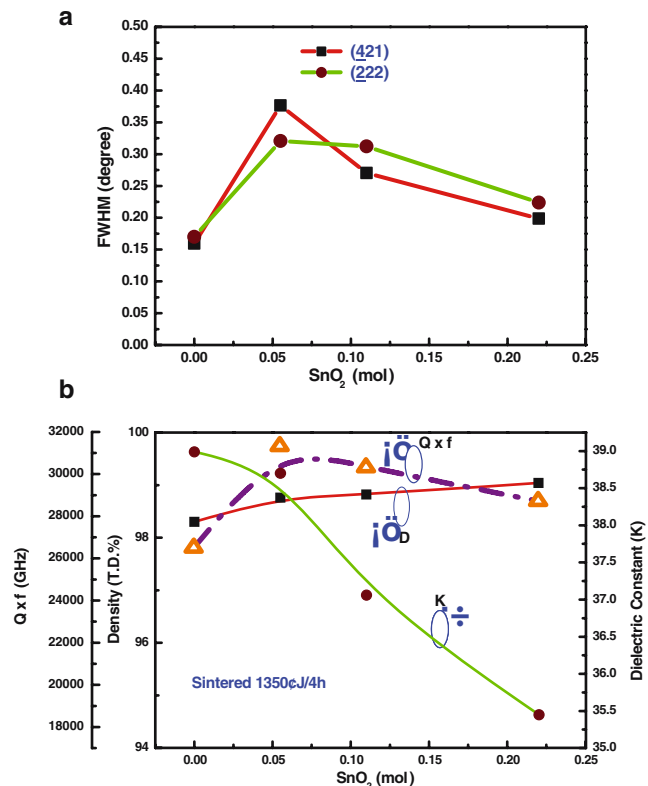


**Fig. 8** Variation of **a** the full-width at half-maximum (FWHM) of the (421) & (222) diffraction peaks with the  $\text{SnO}_2$  content incorporated into the materials and **b** the sintered density,  $D$ , dielectric constant,  $K$ , and quality factor,  $Qxf$ -value, for the  $\text{Ba}_2(\text{Ti}_{9-x}\text{Sn}_x)\text{O}_{20}$  materials ( $x=0.055\text{--}0.220\text{ mol}$ ); The  $\text{Ba}_2(\text{Ti}_{9-x}\text{Sn}_x)\text{O}_{20}$  materials were sintered at  $1,350\text{ }^\circ\text{C}$  (4 h)

It indicates that FWHM first increases for 0.05 mol SnO<sub>2</sub>-doped samples and then decreases for 0.11 and 0.22 mol SnO<sub>2</sub>-doped ones. Larger FWHM in diffraction peaks implies smaller grain size. However, since all the materials contain rod-shaped grains of the same diameter, larger FWHM in diffraction peaks can be attributed to smaller length, i.e., smaller aspect ratio.

The effect of SnO<sub>2</sub>-doping on the characteristics of the 1,350 °C/4 h-sintered Ba<sub>2</sub>Ti<sub>9</sub>O<sub>20</sub> samples are summarized in Fig. 8b, which reveals that the dielectric constant ( $K$ ) for the Ba<sub>2</sub>Ti<sub>9</sub>O<sub>20</sub> monotonously decreases with the proportion of SnO<sub>2</sub>-species incorporation, even though these samples possess a density higher than the undoped ones. The possible explanation is that, in the Ba-Ti(Sn)-O materials made of the corner shared TiO<sub>6</sub>- (or SnO<sub>6</sub>-) octahedrons, the displacement of Ti<sup>4+</sup>-ions in the TiO<sub>6</sub>-octahedrons (or Sn<sup>4+</sup>-ions in the SnO<sub>6</sub>-octahedrons) in respond to the applied electric field is presumed to be the main electrical polarization mechanism, resulting in large dielectric constant. The decreases in  $K$ -value due to SnO<sub>2</sub>-doping can apparently be attributed to the lower polarizability of the Sn<sup>4+</sup>-ions in the SnO<sub>6</sub>-octahedrons, as compared with the Ti<sup>4+</sup>-ions in the TiO<sub>6</sub>-octahedrons. Such a phenomenon is similar to the effect of SnO<sub>2</sub> addition on the low frequency (~10 kHz) dielectric properties of BaTiO<sub>3</sub> perovskite materials.

The mechanism, by which the SnO<sub>2</sub> addition affects the Qxf-value of the Ba<sub>2</sub>Ti<sub>9</sub>O<sub>20</sub> materials is more complicated. On one hand, addition of SnO<sub>2</sub>-species reduces the aspect ratio of the grains, which is beneficial to the densification process and is expected to improve the quality factor for the materials. But, on the other hand, the presence of Sn<sup>4+</sup>-ions in the octahedrons will degrade the coherency of the intrinsic lattice vibration modes, which will impose critical effect on the quality factor for the materials [15, 16]. Figure 8b shows that, for the 1,350 °C/4 h-sintered samples, the quality factor (Qxf) for lightly doped samples (containing 0.05 mol SnO<sub>2</sub>) is better than undoped ones. for example, (Qxf)<sub>SnO<sub>2</sub></sub> = 30,800 GHz for 0.055 mol SnO<sub>2</sub>-doped materials and (Qxf)<sub>undoped</sub> = 26,000 GHz for undoped ones. But the Qxf-value decreases monotonously with increasing concentration of the SnO<sub>2</sub>-species for the heavily doped ones (containing 0.11 or 0.22 mol SnO<sub>2</sub>), such that Qxf-value is lowered to (Qxf)<sub>SnO<sub>2</sub></sub> = 28,600 GHz for 0.22 mol SnO<sub>2</sub>-doped samples. The possible explanation for such a contradictory phenomenon is that, while the addition of small amount of SnO<sub>2</sub>-species facilitates the densification process by suppressing the anisotropic growth of the grains, incorporation of larger amount of SnO<sub>2</sub>-species than necessary will not further improve the granular structure for the Ba<sub>2</sub>(Ti<sub>9-x</sub>Sn<sub>x</sub>)O<sub>20</sub> materials, but will degrade the coherency in lattice vibrational modes for the materials. Therefore, the Qxf-value of the Ba<sub>2</sub>(Ti<sub>9-x</sub>Sn<sub>x</sub>)O<sub>20</sub> materials increased firstly for lightly SnO<sub>2</sub>-doped samples and then it

decreased with the proportion of SnO<sub>2</sub>-species when the SnO<sub>2</sub>-content is abundant. Moreover, Fig. 8a and b indicates that the Qxf-value varies with SnO<sub>2</sub>-content in the same trend as the FWHM does, which implies that the Qxf-value is larger for samples with grains of smaller aspect ratio.

#### 4 Conclusion

The effect of SnO<sub>2</sub> and ZrO<sub>2</sub> addition on the crystal structure and microstructure of the Ba<sub>2</sub>Ti<sub>9</sub>O<sub>20</sub> materials and their related microwave dielectric properties were systematically investigated. The addition of SnO<sub>2</sub> and ZrO<sub>2</sub> increases the densification rate, lowers dielectric constant ( $K$ ), but improves qualify factor (Qxf) of the materials, provided that the materials were not over-fired. The best microwave dielectric properties obtained are ( $K$ )<sub>SnO<sub>2</sub></sub> = 36.5 and (Qxf)<sub>SnO<sub>2</sub></sub> = 31,500 GHz, which occurs for the 0.055 mol SnO<sub>2</sub>-doped and 1,350 °C/4 h sintered samples. These properties are superior to those for the undoped samples [( $K$ )<sub>undoped</sub> = 38.8 and (Qxf)<sub>undoped</sub> = 26,500 GHz]. The possible mechanism is the lowering of the aspect ratio of the Ba<sub>2</sub>(Ti<sub>9-x</sub>Sn<sub>x</sub>)O<sub>20</sub> grains, which facilitates the densification process and improves the microstructure of the materials.

**Acknowledgements** The authors gratefully thank the financial support of the National Science Council, R. O. C. for this research through the project no. NSC 95-2112-M032-005.

#### References

1. G.H. Jonker, W. Kwestroo, J. Am. Ceram. Soc. **41**(10), 390–394 (1958)
2. J.K. Plouide, D.F. Linn, H.M. O'Bryan, J. Thomson, J. Am. Ceram. Soc. **58**(9–10), 418–420 (1975)
3. S. Nomura, Jpn. J. Appl. Phys. **22**(7), 1125–1128 (1983)
4. T. Jaakola, Ceram. Int. **13**, 151–157(1987)
5. K.H. Yoon, J.B. Kim, W.S. Kim, E.S. Kim, J. Mater. Res. **11**(8), 1996–2001 (1999)
6. W.Y. Lin, R.F. Speyer, J. Am. Ceram. Soc. **82**(5), 1207–1211 (1999)
7. J.M. Wu, H.W Wang, J. Am. Ceram. Soc. **71**(10), 868–875 (1988)
8. W.B. Ng, J. Wang, J. Am. Ceram. Soc. **82**(3), 529–534 (1999)
9. R.D. Richtmyer, J. Appl. Phys. **10**, 191–196 (1939)
10. J. Krupka, IEEE Trans. Microwave Theor. Tech. **36**(9), 774–779 (1988)
11. S.G. Mhaisalkar, D.W. Readey, S.A. Akbar, J. Am. Ceram. Soc. **74**(8), 1894–1898 (1991)
12. L.-W. Chu, G.-H. Hsieue, I.-N. Lin, Ferroelectrics, in press (2005)
13. L.-W. Chu, G.-H. Hsieue, I.-N. Lin, J. Am. Ceram. Soc. **88**(12), 3405 (2005)
14. Kajfez D., Guillou P., *Dielectric Resonators* (Artech House, Norwood, MA, 1986), pp. 65–111
15. C.T. Chia, Y.C. Chen, H.F. Cheng, I.N. Lin, J. Appl. Phys. **94**(5), 3360 (2003)
16. Y.C. Chen, H.F. Cheng, H.L. Liu, C.T. Chia, I.N. Lin, J. Appl. Phys. **94**(5), 3365 (2003)